https://doi.org/10.1088/1361-6439/ac4956

Fabrication, modeling, and characterization of soft twisting electrothermal actuators with directly printed oblique heater

Yang Cao^{1,2} and Jingyan Dong^{1,*}

E-mail: jdong@ncsu.edu

Received 12 October 2021, revised 14 December 2021 Accepted for publication 7 January 2022 Published 21 January 2022



Abstract

Soft electrothermal actuators have drawn extensive attention in recent years for their promising applications in biomimetic and biomedical areas. Most soft electrothermal actuators reported so far demonstrated uniform bending deformation, due to the deposition based fabrication of the conductive heater layer from nanomaterial-based solutions, which generally provides uniform heating capacity and uniform bending deformation. In this paper, a soft electrothermal actuator that can provide twisting deformation was designed and fabricated. A metallic microfilament heater of the soft twisting actuator was directly printed using electrohydrodynamic (EHD) printing, and embedded between two structural layers, a polyimide film and a polydimethylsiloxane layer, with distinct thermal expansion properties. Assisted by the direct patterning capabilities of EHD printing, a skewed heater pattern was designed and printed. This skewed heater pattern not only produces a skewed parallelogram-shaped temperature field, but also changes the stiffness anisotropy of the actuator, leading to twisting deformation with coupled bending. A theoretical kinematic model was built for the twisting actuator to describe its twisting deformation under different actuation effects. Based on that model, influence of design parameters on the twisting angle and motion trajectory of the twisting actuator were studied and validated by experiments. Finite element analysis was utilized for the thermal and deformation analysis of the actuator. The fabricated twisting actuator was characterized on its heating and twisting performance at different supply voltages. Using three twisting actuators, a soft gripper was designed and fabricated to implement pick-and-place operations of delicate objects.

Supplementary material for this article is available online

Keywords: soft actuator, electrohydrodynamic (EHD) printing, soft twisting actuator, electrothermal actuator

1

(Some figures may appear in colour only in the online journal)

1361-6439/22/035001+11\$33.00 Printed in the UK

© 2022 IOP Publishing Ltd

¹ Edward P Fitts Department of Industrial and Systems Engineering, North Carolina State University, Raleigh, NC 27606, United States of America

² Industrial and Robotics Engineering Department, Gannon University, Erie, PA 16541, United States of America

^{*} Author to whom any correspondence should be addressed.

1. Introduction

Soft actuators are mainly made of elastomeric or flexible materials. The actuators change their shape or size in response to various stimuli such as electricity [1], heat [2], chemicals [3], light [4], magnetic fields [5], and pneumatic pressure [6]. In the past decade, there has been an increasing interest in the research of soft actuators, due to their lightweight, high flexibility and adaptability, compliance, and compatibility for human-robot interactions. These characteristics give them potential uses in the field of biomimetic applications like artificial muscles [7, 8], biomimetic grippers [9], and soft robotics [10–12]. Soft electrothermal actuators use resistive heating as the stimulus and are usually fabricated in a bimorph structure with two layers that have significantly different coefficient of thermal expansion (CTE). The electrothermal actuators have a conductive heater layer, either as one of the structural layers or as a separate embedded layer, to provide Joule heat to drive the actuator. When the bimorph structure of the actuator is exposed to the temperature change induced by resistive heating, the large mismatch of the thermal expansions between the two structural layers triggers the actuator to bend.

Most soft electrothermal actuators reported so far demonstrated uniform bending deformation, due to the fabrication method of the conductive heater layer using nanomaterial-based solutions. Conventional fabrication methods for the conductive layer of soft electrothermal actuators are mostly deposition-based, such as spin-coating [13], casting [14], filtration [15], and spray [16]. A uniform conductive layer is generally produced from these deposition techniques, which only provides even heating capability and is difficult to realize customized heating distributions and complex deformations other than uniform bending. Twisting represents another degree-offreedom for soft actuators to enhance their versatility and functionality. Generally, twisting deformation requires soft actuators to have controlled non-uniform actuation of the actuator.

Twisting deformation of soft actuators can be achieved from skewed bending deformation, which produces a coupled twisting and bending deformation. When the bending direction of the actuator is misaligned with its longitudinal axis, a twisting deformation can be obtained. One method to achieve twisting deformation is by changing the stiffness anisotropy. Bending deformation tends to occur along the direction with the lowest stiffness. When the actuator has reinforcement structures (reinforcing stripes, fibers, or wires) that change its stiffness anisotropy so that the lowest stiffness direction misaligns with the transverse axis, the actuator tends to bend along this skewed direction with the lowest stiffness, and hence a twisting deformation can be achieved with the coupled bending deformation. For example, Song et al [17] developed a shape memory alloy actuator that can achieve customized bending and twisting actuation. A layered reinforcement structure was embedded in the matrix to vary the mechanical properties of the actuator. When the reinforcement structure is along or perpendicular to the transverse axis, a pure bending deformation is obtained. When the layered reinforcement structure ply configuration is misaligned with the transverse direction by 30/45/60 degree, a twisting deformation can be achieved. Similarly, Wang *et al* [18] designed a thermal responsive soft actuator that exhibits twisting deformation, which comes from its structure anisotropy induced by the embedded shape memory polymer fibers in a homogeneous elastic matrix.

The other commonly used approach to achieve twisting deformation is changing the actuation direction. For soft pneumatic network actuators, this can be done by orienting the air chambers by an angle from the transverse direction. For example, Wang et al [19] reported a soft pneu-net actuator to generate twisting motion with coupled bending, which was achieved by creating oblique air chambers. Through finite element analysis (FEA) and experimental verification, variation trends of bending and twisting motions with respect to the chamber angle were investigated. Some photo responsive materials exhibit uniaxial deformation or have a dominant deformation direction. Hu et al [20] reported a photo actuator which was fabricated by compositing a photo-liquefiable azobenzene derivative with polyethylene film. Guided rubbing and annealing treatments were subsequently applied to the composite film. Actuators obtained by cutting along the rubbing direction exhibited only bending deformation, while actuators obtained by cutting at an angle with the rubbing direction exhibited helical twisting. Haan et al [21] reported humidity responsive actuators based on a single sheet of a hydrogenbonded, uniaxially aligned liquid crystal polymer network. The asymmetry in the molecular trigger in the anisotropic polymer film plays a dominant role leading to programmed deformations including bending, folding, and twisting.

More dedicated twisting deformation with little coupled bending can be achieved by combining two perpendicular straining deformations, as the opposite bending deformations cancel out. For example, Grinberg et al [22] developed a piezoelectric beam actuator driven by interdigitated electrodes (IDEs), deposited over its top and bottom surfaces. IDEs on both top and bottom surfaces have a 45° angle with the beam axis but orient at the opposite directions. When only one set of electrodes is actuated, either on the top or bottom surface, a coupled bending and twisting response is induced. However, if both the top and bottom electrodes are actuated, a pure twisting mode can be achieved. Wang et al [23] developed a dual-layer liquid crystal soft actuator that can bend under ultraviolet irradiation and twist under near-infrared irradiation. The top layer possesses a uniaxially aligned liquid crystalline elastomer matrix incorporated with azobenzene chromophores and a near-infrared absorbing dye, so it bends under ultraviolet stimulus and shrinks under near-infrared stimulus. The bottom layer has only near-infrared dye, and only responds to near-infrared stimulus. Because the shrinkage directions of the top and bottom layers are tilted to each other, the actuator executes twisting deformation under near-infrared irradiation. Similarly, Finio et al [24] developed a piezoelectric twisting actuator by deploying antisymmetric top and bottom fiber-reinforced composite layers. Gorissen et al [25] fabricated a pneumatic twisting actuator by combining two arrays of pneumatic balloon actuators with opposite bending directions.

In this paper, a soft twisting electrothermal actuator was designed, fabricated, and characterized. The conductive metallic microfilament heater of the actuator was directly printed in a skewed orientation using the electrohydrodynamic (EHD) printing technology. EHD printing was selected as the fabrication method due to its high-resolution direct patterning capabilities and simpler processing than lithography and etching based technologies. Meanwhile, a low melting point alloy is used and directly printed as the heating element, which has higher conductivity than most conductive composites used in common ink-printing techniques. The resistive heater was embedded in the two structural layers of polyimide (PI) and polydimethylsiloxane (PDMS), which are selected due to their largely different CTEs. This skewedly oriented heater filament not only creates a skewed parallelogram-shaped temperature field, but also changes the mechanical anisotropy of the actuator, which leads to twisting deformation with coupled bending. A theoretical kinematic model was built to describe its twisting deformation under different actuation effects. Based on the theoretical model, the effect of the design parameters on the resulting twisting angle and motion trajectory of the twisting actuator were studied and compared with experimental results. FEA simulation tool was utilized for the thermal and deformation analysis. The fabricated soft twisting actuator has been characterized on its heating and twisting performance at different actuation voltages. Using three twisting actuators, a soft gripper was designed and fabricated to implement pickand-place operations of delicate objects.

2. Fabrication of the twisting electrothermal actuator

The soft actuator was designed with a bimorph structure with embedded microfilament heater fabricated by EHD printing using a low melting point alloy. The two structural layers of the bimorph structure are PI and PDMS due to the large mismatch of their thermal expansion capabilities. The CTEs of PI and PDMS are $20 \times 10^{-6}~^{\circ}\text{C}^{-1}$ and $320 \times 10^{-6}~^{\circ}\text{C}^{-1}$, respectively. The heating filament of the soft actuator was directly printed and embedded in-between the PI and PDMS layers using a low melting point solder (Bi58/Sn42, 58% Bismuth and 42% Tin with a melting point of 138 °C, purchased from Qualitek).

An EHD printing process of the low melting point metal ink was developed for the fabrication of the embedded heater in the actuator [26–28]. As shown in figure 1(a), the EHD printing system consists of four components: a three axes motion stage, a heating syringe, a pneumatic dispensing system, and a high voltage power supply. The motion stage, directed by computer numerical control program, can move in *XYZ* directions with high precision. A temperature-controlled syringe was heated up to 260 °C to melt the low melting point alloy to increase the ink flowability. A small pressure of 0.1–0.2 psi (689–1379 Pa) was used in the pneumatic dispensing system to ensure a stable flow of the molten metal to the nozzle tip. A high voltage about 2 kV was applied between the nozzle and the ground electrode below the printing substrate to provide

the needed electrostatic force for printing. When the resulting electrostatic force overcomes surface tension of the ink, the ink meniscus at the nozzle tip forms a conical shape (i.e. Taylor cone), and a fine filament whose size is smaller than the nozzle's diameter is ejected onto the substrate.

To fabricate the soft twisting actuator, a layer of PDMS was first coated on a glass slide. The microfilament heater was then printed on the cured PDMS substrate by EHD printing. The printed heater filaments have a semi-circle profile with a diameter (i.e. linewidth) about 100 μ m and a height about 50 μ m. Then, a PI tape (with a 25.4 μ m thick PI layer and a 25.4 μ m silicone adhesive layer) was pressed against the printed heater to peel the heater filament off from the PDMS substrate. Thereafter, copper wires were connected to the printed heater using solder for electrical connection to the power supply. Finally, a layer of PDMS was blade coated to seal the microfilament heater in between the PDMS and the PI layer with controlled PDMS layer thickness (about 250 μ m). The thickness was controlled by a gap between the coating blade and substrate, which was set by laying two plastic films with pre-determined thickness. The top PDMS layer was cured at room temperature (to minimize the residue thermal stress) for 24 h, then the actuator was produced by cutting the bimorph film into designed sizes (10 mm by 40 mm rectangular shape for the actuator in figure 1(b)).

In our previous research [29-31], we have studied soft electrothermal actuators with uniform bending and the general design concepts for programmable deformations. In this work, we specifically focused on the design, kinematic modeling, and FEA of soft electrothermal actuators that demonstrated twisting deformation. Unlike the uniform bending actuator, the twisting actuator was designed with a skewedly oriented heater pattern, as shown in figure 1(b). This oblique heater pattern not only produces a parallelogram high temperature area, but also changes the stiffness anisotropy of the actuator. For the previous uniform bending heater pattern, the temperature distribution is approximately even, and the transverse direction has the lowest bending stiffness. While for the skewed heater pattern, the heating area and the direction with the lowest bending stiffness shifts to be parallel to the skewed heater filaments, as shown in figure 1(c). The actuator tends to bend along this oblique direction, resulting in the twisting deformation with coupled bending (figure 1(d)). It is worthy to point out that both skewed heating area and mechanical anisotropy contribute to the overall twisting deformation. It was observed that an actuator with skewed heater filaments but filling in a rectangular shape showed only around half of the twisting angle of the twisting actuator with a parallelogram shaped heater at the same voltage. Therefore, both features are adopted in the design of this work to achieve maximum twisting deformation.

3. Modeling of the deformation of the twisting actuator

The soft twisting actuator provides much more complicated deformation, compared with uniform bending actuators. It

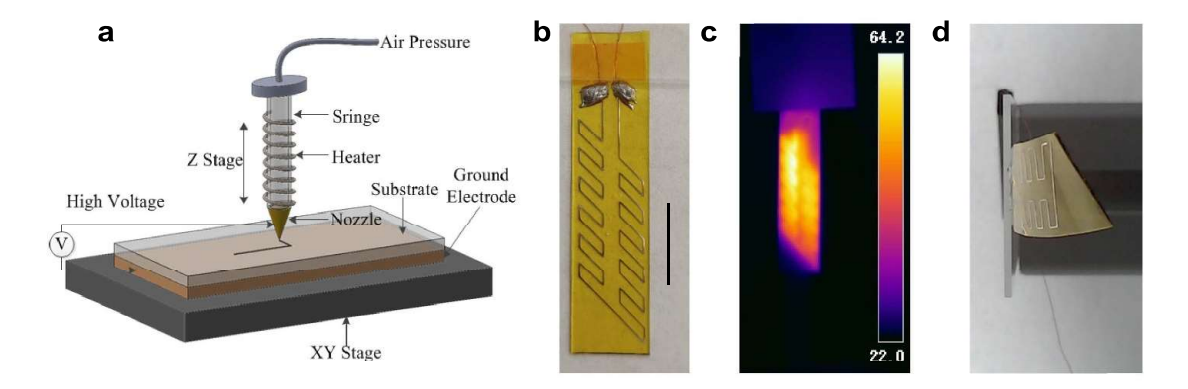


Figure 1. (a) The schematic EHD printing system. (b) A fabricated twisting electrothermal actuator with EHD printed skewed heater filaments (scale bar is 10 mm). (c) Thermography of an actuated soft twisting actuator showing skewed parallelogram temperature distribution. (d) The actuator produces twisting deformation along with coupled bending.

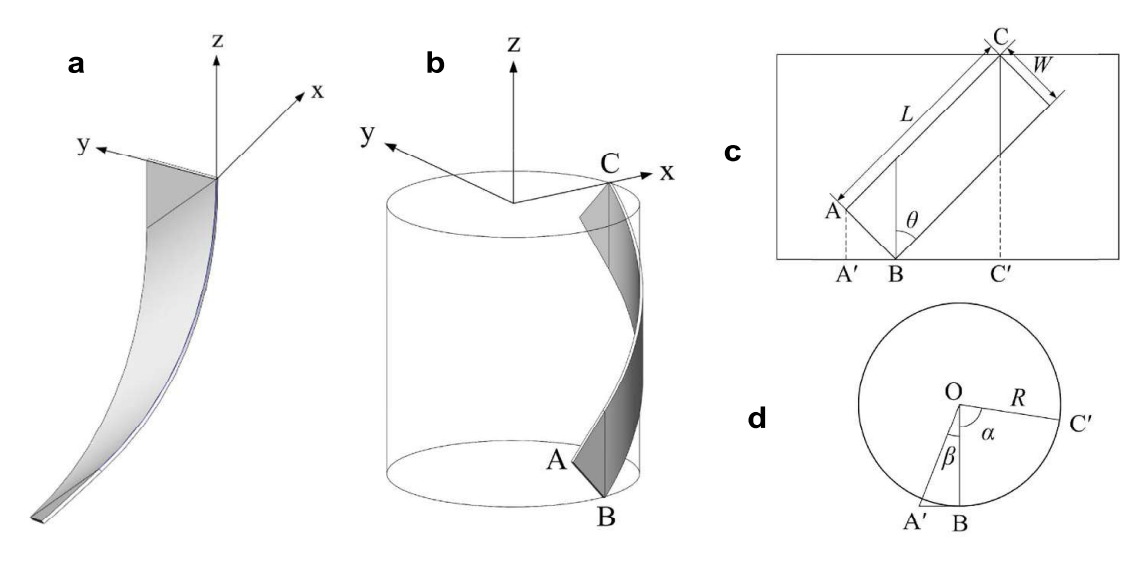


Figure 2. (a) The original coordinate system of the twisting actuator. (b) The transformed coordinate system to calculate position of the free end. (c) Development of the reference cylinder and the actuator. (d) Projection of points on the actuator to the cylinder bottom.

is very important to understand the relationship between the actuation voltage, the curvature of the oblique bending, and the resulting twisting angle and the free end position, so as to apply the twisting actuator in delicate applications, such as soft robotics. For the soft actuator designed in this work, due to the skewed temperature distribution and stiffness anisotropy, actuators with a skewed heater pattern exhibit twisting deformation with coupled bending when actuated with electricity. This coupled twisting and bending deformation is resulted from a bending deformation that misaligns the transverse direction. Assuming the structural deformation of the actuator comes from the parallelogram-shaped heated area, the rectangular actuator can be divided into three segments, a parallelogram segment and two triangle segments, as shown in figure 2(a). The parallelogram segment undergoes skewed bending deformation, while the two triangle segments mostly remain tangent to the parallelogram segment since their temperature does not increase significantly during the actuation.

Figure 2(a) shows the actuator in the original rectangular coordinate system, but it is difficult to use this coordinate system for theoretical modeling and calculation. Since bending of the parallelogram-shaped heated area is along the skewed direction, if the bending curvature is known, the actuator will wrap around a cylinder with its z-axis being parallel to the skewed direction and its radius being the same to the bending radius of the actuator. Therefore, a transformed cylindrical coordinate system as shown in figure 2(b) is used for modeling the deformation of the actuator. In the cylindrical coordinate system, Z-axis is the reference axis and X-axis is the reference direction. Assume that the top edge of the actuator is fixed, and the bottom edge is free to move. In order to find the bottom edge's position and the twisting angle, we need to calculate the coordinates of points A and B (as shown in figure 2(b)). The reference cylinder and the wrapped actuator can be laid out on a surface as shown in figure 2(c). In figure 2(c), L and W are length and width of the actuator, θ

is the heater pattern inclination angle with respect to the longitudinal direction. Also, points on the actuator can be projected to the bottom of the cylinder as shown in figure 2(d), in which A' and C' are projections of A and C, and R is radius of the cylinder $(R=1/\kappa, \text{ where } \kappa \text{ is the bending curvature})$ of the actuator). Based on these two diagrams, the axial distance of point A is L $OA' = \sqrt{R^2 + W^2 \cos^2 \theta}$, its azimuth is equal to angle $-(\alpha + \beta) = -\frac{\sin\theta(L - W \cot\theta)}{R} - \tan^{-1}\frac{W \cos\theta}{R}$, and the height is $-L\cos\theta$. For point B, axial distance is R, azimuth is angle $-\alpha = \frac{\sin\theta(L - W \cot\theta)}{R}$, and height is $-L\cos\theta - W \sin\theta$. Coordinates of points A and B are summarized below.

$$A(\rho, \varphi, z) = \left(\sqrt{R^2 + W^2 \cos^2 \theta} - \frac{\sin \theta (L - W \cot \theta)}{R} - \tan^{-1} \frac{W \cos \theta}{R} - L \cos \theta\right), \tag{1}$$

$$B(\rho,\varphi,z) = \left(R - \frac{\sin\theta(L - W\cot\theta)}{R}, -L\cos\theta - W\sin\theta\right). \tag{2}$$

Cylindrical coordinates then can be transformed into rectangular coordinates in the calculation coordinate system:

$$x = \rho \cos \varphi, \tag{3}$$

$$y = \rho \sin \varphi, \tag{4}$$

$$z = z. (5)$$

The rectangular coordinates in the calculation coordinate system can be converted into the original rectangular coordinate system by transformation of the coordinate system. This can be done by two steps: translate along x-axis by length R, and rotate around x-axis by $-\theta$ (negative sign means a clockwise direction). Afterwards, we are able to find the coordinates of A and B in the original coordinate system using the following equation:

$$\begin{bmatrix} x' \\ y' \\ z' \end{bmatrix} = \begin{bmatrix} 1 & 0 & 0 \\ 0 & \cos(-\theta) & \sin(-\theta) \\ 0 & -\sin(-\theta) & \cos(-\theta) \end{bmatrix} \begin{bmatrix} x \\ y \\ z \end{bmatrix} - \begin{bmatrix} R \\ 0 \\ 0 \end{bmatrix}.$$
(6)

Twisting angle of the free edge can be obtained by calculating the angle between line AB's projection on X-Y plane and Y-axis:

$$TA = \tan^{-1} \left(\frac{x'(B) - x'(A)}{y'(B) - y'(A)} \right). \tag{7}$$

Based on the constructed model, design parameters including actuator L, W, bending curvature (κ) , and heater pattern inclination angle (θ) all affect the twisting angle. These design parameters can be integrated in the process of device fabrication to optimize actuator design and achieve desired response. Figure 3(a) shows the relationship between twisting angle and

actuator length when other parameters are set as W = 10 mmand $\theta = 45^{\circ}$. Theoretically, twisting angle is proportional to the actuator length. We fabricated four actuators whose length ranged from 17 to 62 mm and measured their twisting angles when the bending curvature was approximately 0.3 cm⁻¹ under actuation. As we can see from figure 3(a), the experimental results generally agree well with the trend from the theoretical model. From figure 3(b), the twisting angle is inversely proportional to the actuator width, in which actuator length is set to 32 mm and heater pattern inclination angle is 45°. We fabricated three actuators whose widths were 5, 10, and 15 mm, and measured their twisting angles when the bending curvature was approximately 0.3 cm⁻¹. The twisting angle generally decreases as the actuator width increases, following the theoretical trend. Intuitively, the twisting angle is proportional to the bending curvature of the actuator, which is confirmed in figure 3(c). When the actuator length is fixed to 32 mm and actuator width is fixed to 10 mm, twisting angle is proportional to the bending curvature as shown in figure 3(c). Twisting angle at different bending curvatures was measured, which agrees with the theoretical trend. Lastly, the relationship between twisting angle and the inclination angle of the heater pattern is presented in figure 3(d), in which actuator length is 32 mm and actuator width is 10 mm. Note that on the horizontal axis in figure 3(d), the heater pattern inclination angle starts from 17.35°, which is the smallest heater inclination angle when the actuator length is 32 mm and actuator width is 10 mm based on our heater pattern configuration. We fabricated three actuators whose heater pattern inclination angles were 30°, 45°, and 60°, and measured their twisting angles when the bending curvature was approximately 0.3 cm⁻¹. When all other design parameters are fixed, the largest twisting angle will be achieved when the heater inclination angle is around 45°. This is quite intuitive as when the inclination angle gets close to 0 or 90°, the deformation will mostly be pure bending deformation.

From the model, we can obtain the coordinates of the two points on the free edge of the actuator, by which we are able to calculate the position of the free edge (shown in figure 4(a)). The displacement of the midpoint on the free edge can be derived by calculating its coordinate change with respect to its original position (0, W/2, -L). Then its displacements in X, Y, and Z directions are:

$$\Delta x = \frac{x'(A) + x'(B)}{2},\tag{8}$$

$$\Delta y = \frac{y'(A) + y'(B)}{2} - \frac{W}{2},\tag{9}$$

$$\Delta z = \frac{z'(A) + z'(B)}{2} + L.$$
 (10)

The theoretical displacement trend of the midpoint on the free edge in X, Y, and Z directions is shown in figure 4(b), in which the actuator length is 32 mm and width is 10 mm, heater pattern inclination angle is 45°. Figure 4(c) shows the motion trajectory of the free edge when the actuator's bending

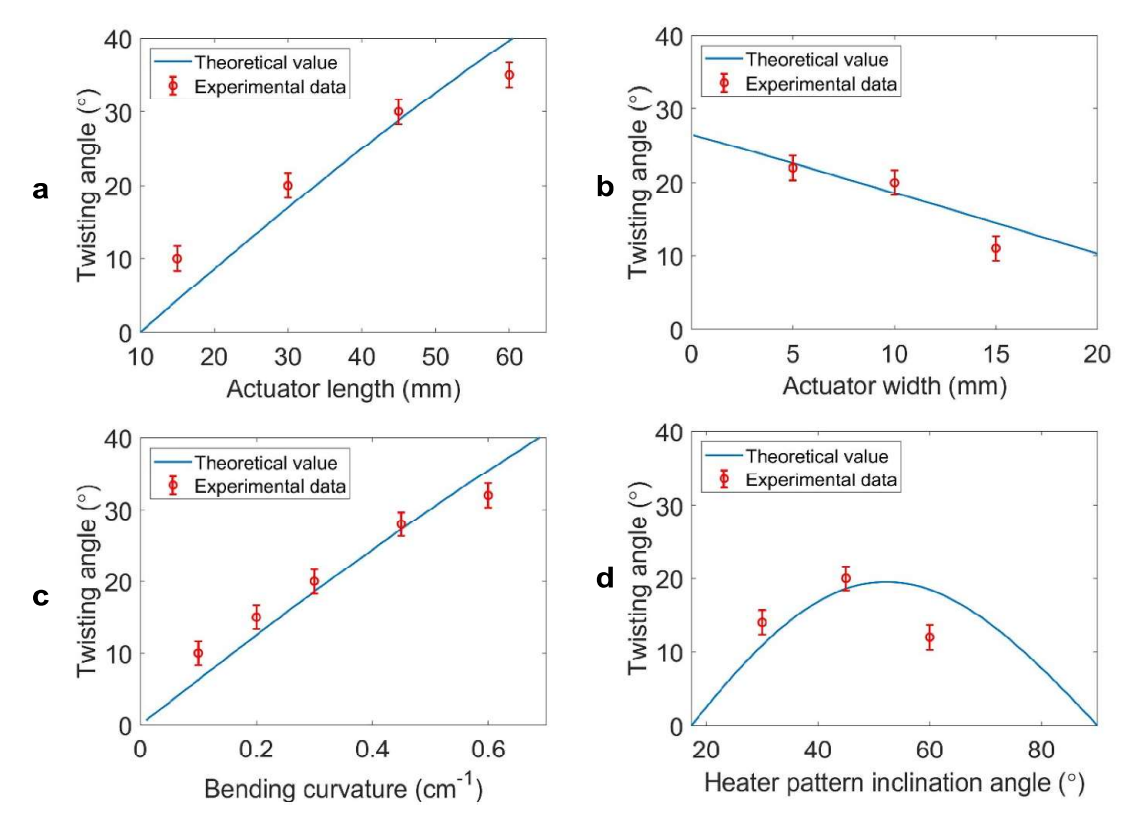


Figure 3. (a) The relationship between twisting angle and actuator length. (b) The relationship between twisting angle and actuator width. (c) The relationship between twisting angle and bending curvature. (d) The relationship between twisting angle and inclination angle of the heater pattern.

curvature gradually increases from 0 to 1 cm⁻¹, and figure 4(d) shows its bottom view, which indicates a trend similar to the sequential images we obtained experimentally in the next section.

4. FEA of the soft electrothermal actuator

To help the design of the soft twisting actuator, FEA simulation is used to study the temperature distribution and deformation of the twisting actuator. Our electrothermal actuator is a coupled multi-physical system with electric-thermalmechanical responses. FEA is a powerful tool to simulate and analyze the actuation process and the relationship between supply voltage, temperature distribution, and deformation. A 3D model was generated by SolidWorks and then SolidWorks part files were converted to Parasolid files that can be imported into FEA software ANSYS. In the CAD model, the actuator was simplified to a bilayer structure, in which the silicone adhesive layer was added to the PDMS silicone layer due to their similar physical properties. The simulation work consists of two analysis systems: a thermal-electric system and a static structural system. The two analysis systems share the same engineering data and geometry information, and the solution results of thermal-electric system is used as input load for the static structural system. All engineering data used is listed in table 1, which come from technical data sheets or scientific papers. Note that we assume the Young's modulus of Bi58/Sn42 decreases linearly from 39 GPa to 0 as the temperature increases from 20 °C to 138 °C (its melting point).

In the meshing process, the element size was set to about 0.3–0.5 mm. Three meshing methods were used. Tetrahedron meshing was used for the PDMS layer, hexahedron meshing was used for the PI layer, and sweep meshing was used for the Bi58/Sn42 filament heater. Meshing methods were selected mainly based on the geometrical features of the object. The PI film has a uniform thickness, so it can be meshed using the hexahedron meshing method. The heater filament has a semi-circular cross-section, and hence a sweep meshing is appropriate. Since the heater filament is embedded inside the PDMS layer, a tetrahedron meshing method is applied to the PDMS layer. To ensure reasonable simulation results and to prevent the three layers from separating each other, topology was shared on the meshing boundaries.

In the thermal-electric system, voltages were applied on the two ends of the heater filament. A constant air convection coefficient 2×10^{-5} W mm⁻² °C was applied on the outside surface of the actuator. For the static structural system, the left edge of the actuator was fixed, while all the other sides were free to deform.

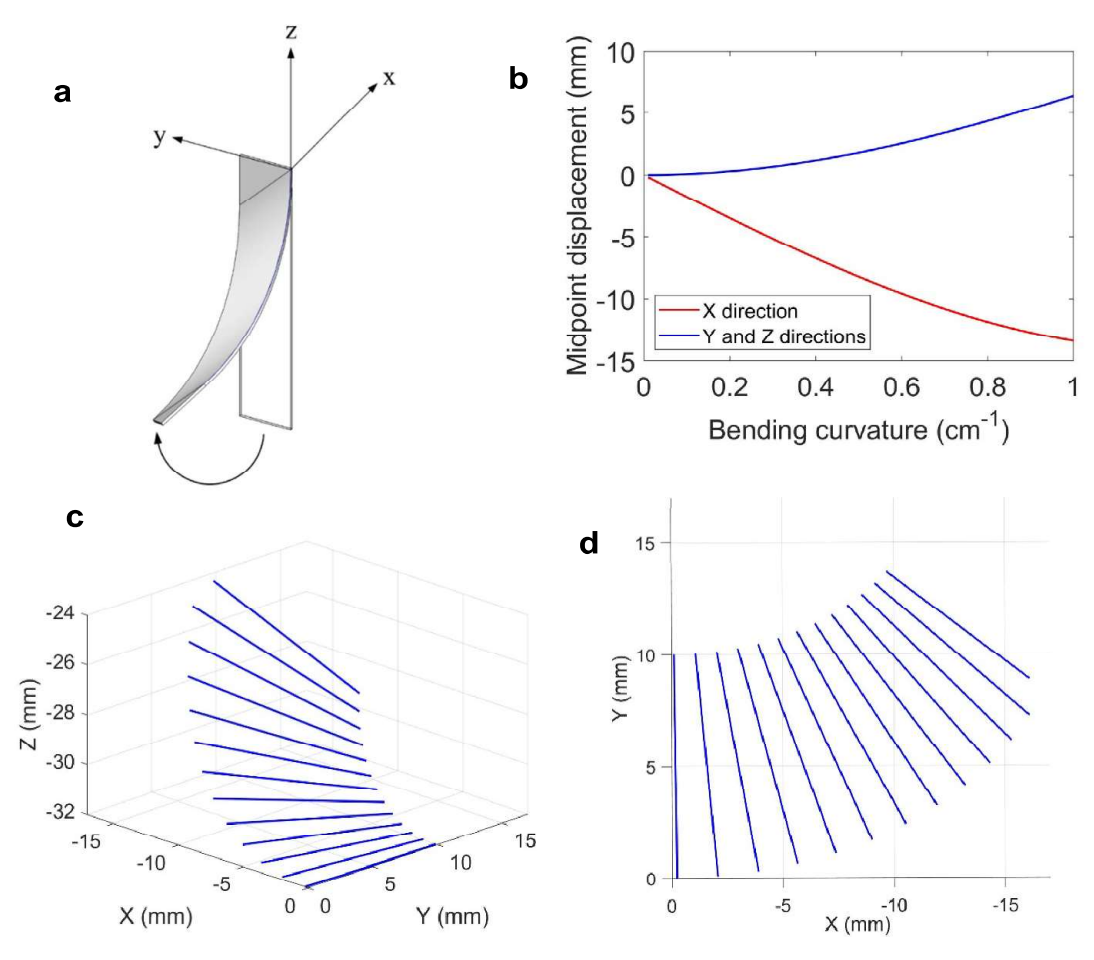


Figure 4. (a) Displacement of the free edge. (b) Displacement of the midpoint on the free edge in x, y, and z directions. (c) Motion trajectory of the free edge. (d) Bottom view of the motion trajectory of the free edge.

Table 1. Engineering data used in the FEA simulation.

Properties	Bi58/Sn42	PDMS	ΡI
Density (kg m ⁻³)	8720	965	1420
Young's modulus (MPa)	39 000–0 ^a	2.6	2500
Poisson's ratio	0.35	0.495	0.34
CTE (ppm/ C°)	16.7	320	20
Thermal conductivity	21.6	0.27	0.12
$(\operatorname{Wm} K^{-1})$			
Specific heat $(J g^{-1})$	46	1.46	1.09
Electrical conductivity	34.5	N/A	N/A
(µohm cm)			

^a Decreases linearly as temperature increases.

The soft electrothermal actuator is generally made of elastic materials, and can generate large deformation when being actuated. Due to its high nonlinearity, simulation of elastic materials is much more difficult than the conventional rigid structures. The elements could become so distorted that the solver cannot give a solution. To overcome the convergence

difficulties under large structural deformation for the soft actuator, a nonlinear adaptive region was used in ANSYS, which commands ANSYS to automatically re-mesh the model or a portion of the model when elements become excessively distorted. Moreover, a semi-implicit solving scheme was applied when the default implicit solver was having trouble, as the semi-implicit solver can better handle very large deformation. As a result, the force and displacement were able to converge even under large deformation.

Based on the CAD model and simulation environment configurations, the thermal analysis and deformation analysis of the soft twisting actuator were studied at different actuation voltages (e.g. 1, 2, 3, and 3.5 V) as shown in figure 5. Clearly for our oblique heater design, a roughly parallelogram heating area and temperature distribution can be observed from the thermal analysis. Twisting deformation can be achieved at the free end of the actuator. The resulting temperature on the actuator and twisting deformation can be controlled by the applied actuation voltage. As shown in the next section, the FEA results are very close to the experimental results shown in figure 6.

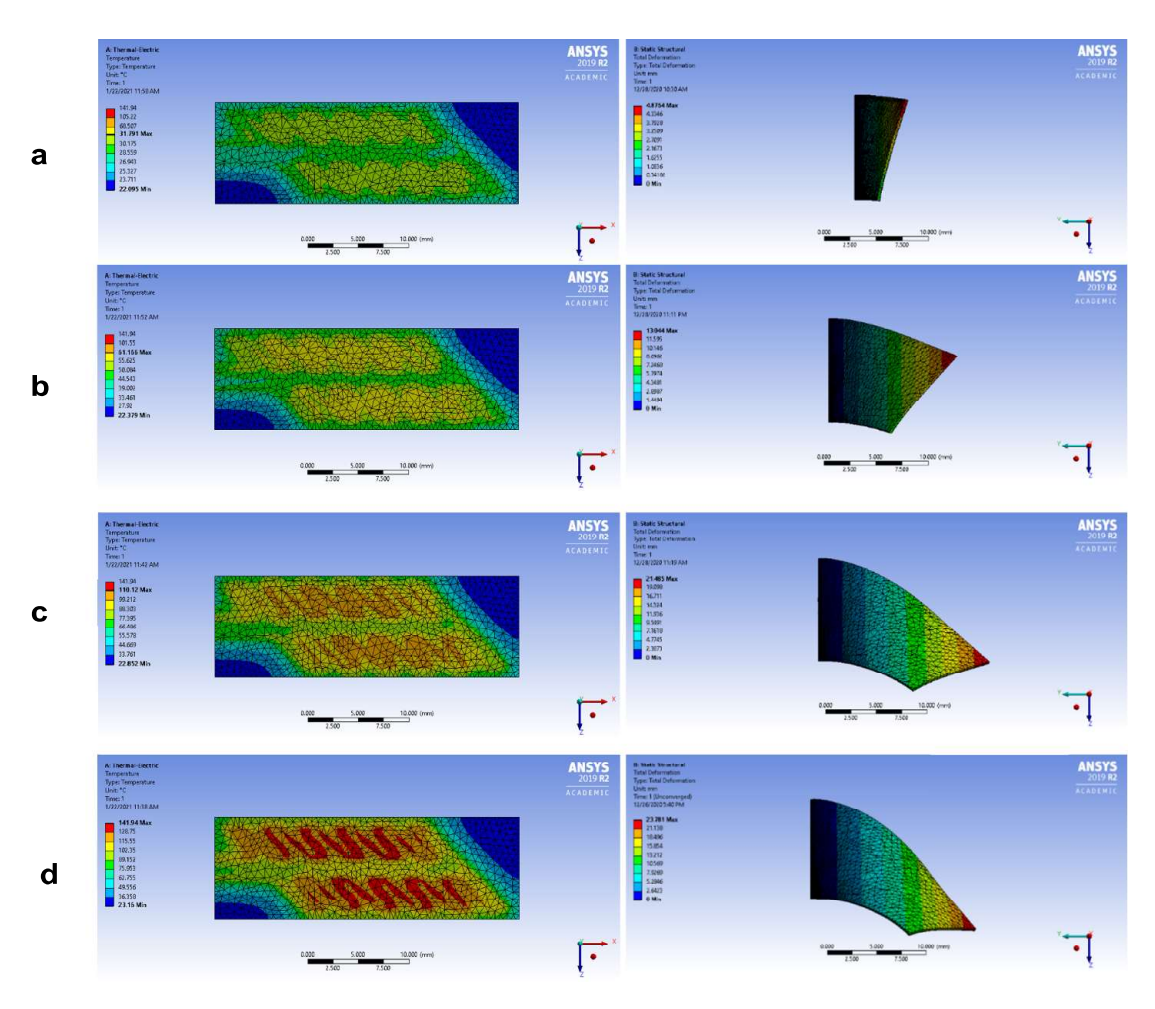


Figure 5. Thermal analysis and deformation analysis of the twisting actuator when the supply voltage is (a) 1 V; (b) 2 V; (c) 3 V; (d) 3.5 V.

5. Experimental characterization of the twisting electrothermal actuator

The fabricated twisting actuator was characterized on its heating and twisting performance at different actuation voltages. Temperature distribution on the twisting actuator was measured by an infrared camera (Fotric 225). Figure 6(a) shows its thermographies at different actuation voltages. Clearly, a parallelogram high temperature zone was observed. Note that the actuator was restrained from deformation when being measured for temperature. Figure 6(b) shows the actuator's twisting deformation at different actuation voltages, in which twisting deformation can be observed with coupled bending. Both figures 6(a) and (b) were captured at steady state when heating had saturated after supplying voltage for more than 1 min. The experimental temperature distribution and twisting deformation of the soft actuator at different actuation voltages are very close to the FEA simulation results in figure 5. Moreover, the motion trajectory of the free edge at different voltages in figure 6(b) resembles the trend of the theoretical model, as shown in figure 4. At 3 V supply voltage, the actuator can generate a torque that is about two times its own weight-length (70 mN mm).

The actuator was also characterized on its heating performance and twisting deformation with regard to the applied electrical voltage. The actuator's average temperature in the parallelogram area and its twisting angle at different actuation voltages were measured, as shown in figures 6(c) and (d), respectively. The actuator's average temperature in the parallelogram area and its twisting angle at different actuation currents are provided in figure S1 (available online at stacks.iop.org/JMM/32/035001/mmedia) in the supplementary information. Linear relationship is observed between the actuation voltage and the resulting twisting angle. Figure 6(e) shows change of the twisting angle as a function of time when a 2.5 V voltage was applied at 0 s while cut off at 60 s. The twisting angle was measured every 5 s by a protractor on the captured image. Specifically, motion of the moving edge of the twisting actuator was first captured by a digital camera. Then the twisting angle was obtained by measuring the rotating angle of the moving edge. Generally, the twisting angle of the actuator increased rapidly when the voltage was applied, and then gradually reached a stable twisting angle within 60 s. Upon turning off the voltage, the twisting angle dropped sharply at the beginning, then decreased slowly to about 5° within 60 s (less than 3° within 90 s, which is a

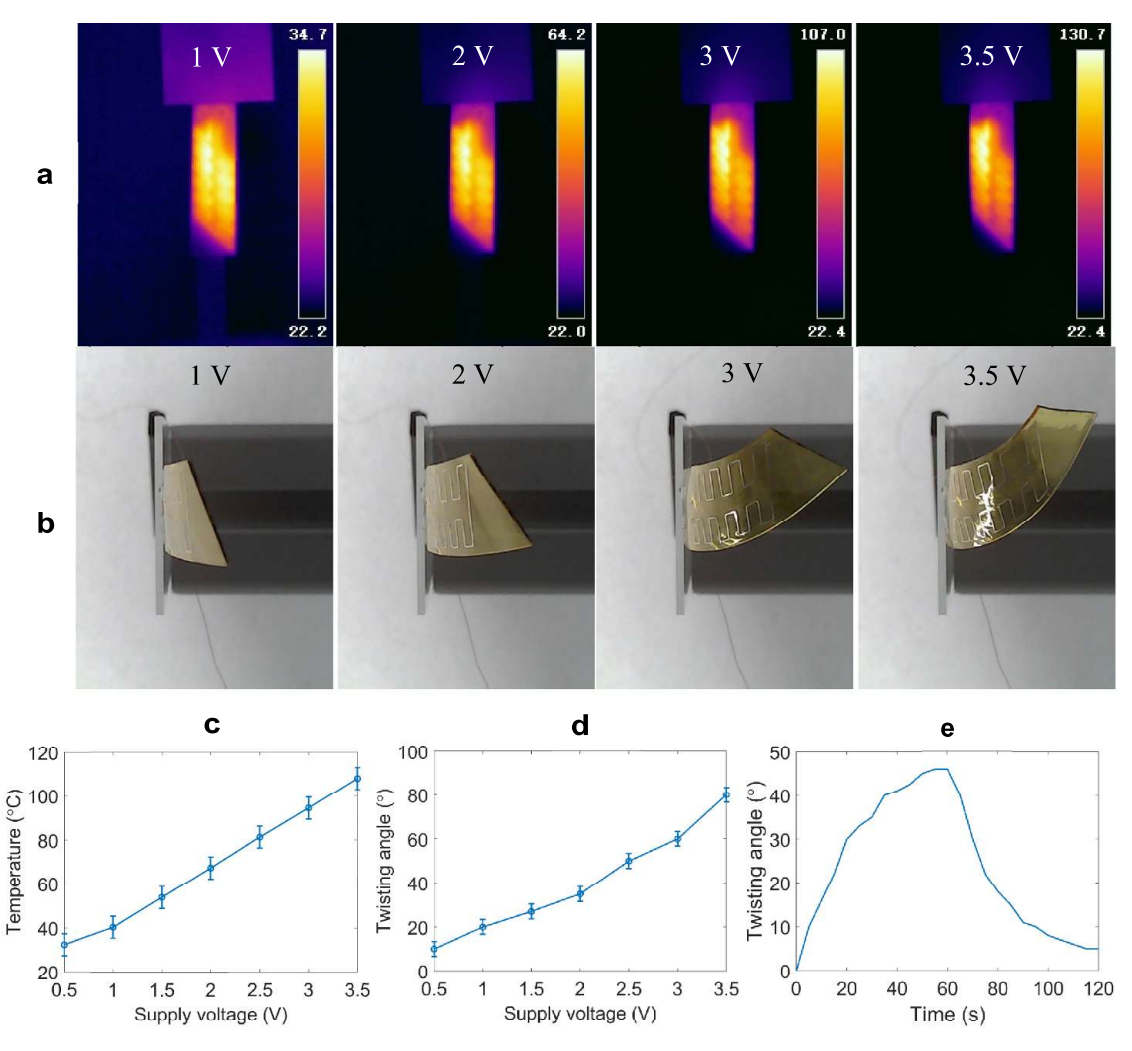


Figure 6. (a) Thermographies and (b) deformation of the twisting electrothermal actuator at different actuation voltages. (c) The measured average temperature in the parallelogram heated area at different voltages. (d) The twisting angle at different voltages. (e) Change of the twisting angle as a function of time when a 2.5 V voltage was applied at 0 s, and cut off at 60 s.

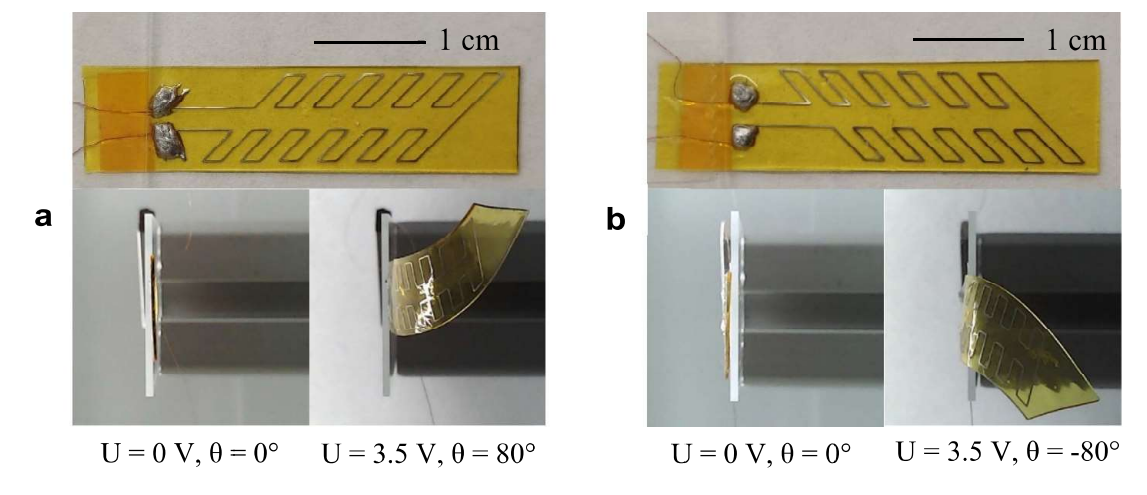
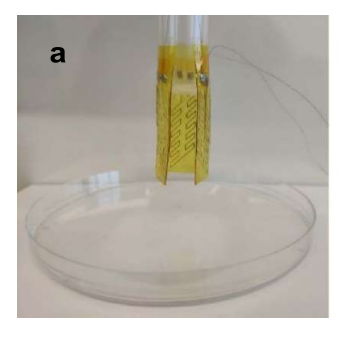
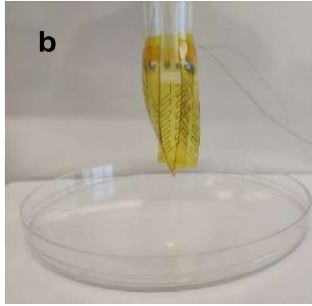


Figure 7. (a) A right skewed heater pattern and counterclockwise twisting. (b) A left skewed heater pattern and clockwise twisting.





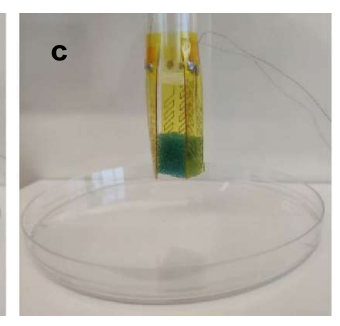


Figure 8. A soft gripper made of three twisting actuators. (a) Initial unactuated state; (b) actuated without load; (c) gripping the sample.

residual angle after actuation). The asymmetric actuation in the heating and cooling stages was caused by the change of the heater's electrical resistance and heat dissipation speed at different temperature, while the residual angle is mainly due to the elastic hysteresis of the silicone materials. Moreover, both clockwise and counterclockwise twisting deformation can be obtained by changing the orientation of the heater filaments. An actuator with right oriented heater pattern exhibits counterclockwise twisting deformation (shown in figure 7(a)), while an actuator with left oriented heater pattern exhibits clockwise twisting deformation (figure 7(b)). Both actuators can achieve an 80° twisting angle when the supply voltage is 3.5 V.

Soft grippers are typical applications of soft actuators, because of their large deformation and gentle interaction with the objects. In this work, three twisting actuators were integrated into a soft gripper to pick-and-place delicate objects. Compared with conventional soft grippers consisting of bending actuators, grippers made of twisting actuators have higher adaptability, and can grasp objects more securely with less gripper fingers. Figure 8 shows a soft gripper made of three twisting actuators. The three twisting actuators were connected in a series circuit. When the actuators were unactuated, the gripper fingers remained flat (shown in figure 8(a)). After applying a voltage, the actuators twisted, and their tips got closer to each other (shown in figure 8(b)). We used a foam block as the gripping sample to mimic a delicate object. As shown in figure 8(c), the soft gripper can securely grasp the sample, which realized humanoid motion without any additional mechanical components and can potentially be used as robotic 'hand' to handle fragile objects that cannot be handled by conventional rigid grippers.

6. Conclusions

In this paper, a soft twisting electrothermal actuator was designed, fabricated, and characterized. The actuator has a bimorph structure with two structural layers (PI and PDMS) having distinct thermal expansion properties, and an EHD printed metallic microfilament heater embedded between the two structural layers. The metallic heater filaments were directly printed in a skewed orientation, which not only produces a skewed parallelogram-shaped high temperature area, but also changes the stiffness anisotropy of the actuator, leading to twisting deformation with coupled bending. A theoretical

geometric model was built for the soft twisting actuator to study the influence of design parameters and the actuation effect on the resulting twisting angle and the deformation of the actuator, which were validated by experiments. FEA simulation using ANSYS was utilized for the thermal analysis and deformation analysis of the twisting actuator. The fabricated twisting actuator was characterized on its heating and twisting performance at different actuation voltages. Using the twisting actuators, a soft gripper was integrated to implement pick-and-place operations of delicate objects.

Data availability statement

All data that support the findings of this study are included within the article and the supplementary information.

Acknowledgments

The authors would like to acknowledge the financial support from the National Science Foundation (NSF) through Award CMMI 1728370.

ORCID iDs

Yang Cao https://orcid.org/0000-0001-9209-3897 Jingyan Dong https://orcid.org/0000-0003-2224-9168

References

- Jun K, Kim J and Oh I K 2018 An electroactive and transparent haptic interface utilizing soft elastomer actuators with silver nanowire electrodes Small 14 1801603
- [2] Kim T H, Choi J G, Byun J Y, Jang Y, Kim S M, Spinks G M and Kim S J 2019 Biomimetic thermal-sensitive multi-transform actuator Sci. Rep. 9 7905
- [3] Zhao Q, Dunlop J W C, Qiu X L, Huang F H, Zhang Z B, Heyda J, Dzubiella J, Antonietti M and Yuan J Y 2014 An instant multi-responsive porous polymer actuator driven by solvent molecule sorption *Nat. Commun.* 5 4293
- [4] Huang C L, Lv J A, Tian X J, Wang Y C, Yu Y L and Liu J 2015 Miniaturized swimming soft robot with complex movement actuated and controlled by remote light signals Sci. Rep. 5 17414
- [5] Schmauch M M, Mishra S R, Evans B A, Velev O D and Tracy J B 2017 Chained iron microparticles for

- directionally controlled actuation of soft robots *ACS Appl. Mater. Interfaces* **9** 11895–901
- [6] Ge L S, Dong L T, Wang D, Ge Q and Gu G Y 2018 A digital light processing 3D printer for fast and high-precision fabrication of soft pneumatic actuators Sens. Actuator A 273 285–92
- [7] Feinberg A W, Feigel A, Shevkoplyas S S, Sheehy S, Whitesides G M and Parker K K 2007 Muscular thin films for building actuators and powering devices *Science* 317 1366–70
- [8] Aliev A E *et al* 2009 Giant-stroke, superelastic carbon nanotube aerogel muscles *Science* **323** 1575–8
- [9] Hu Y, Lan T, Wu G, Zhu Z C and Chen W 2014 A spongy graphene based bimorph actuator with ultra-large displacement towards biomimetic application *Nanoscale* 6 12703–9
- [10] Zheng W J, An N, Yang J H, Zhou J X and Chen Y M 2015 Tough Al-alginate/poly (N-isopropylacrylamide) hydrogel with tunable LCST for soft robotics ACS Appl. Mater. Interfaces 7 1758–64
- [11] Xiao P S, Yi N B, Zhang T F, Huang Y, Chang H C, Yang Y, Zhou Y and Chen Y S 2016 Construction of a fish-like robot based on high performance graphene/PVDF bimorph actuation materials Adv. Sci. 3 1500438
- [12] Shepherd R F, Ilievski F, Choi W, Morin S A, Stokes A A, Mazzeo A D, Chen X, Wang M and Whitesides G M 2011 Multigait soft robot *Proc. Natl Acad. Sci. USA* 108 20400–3
- [13] Sang W, Zhao L M, Tang R, Wu Y P, Zhu C H and Liu J 2017 Electrothermal actuator on graphene bilayer film *Macromol. Mater. Eng.* 302 1700239
- [14] Sun Y C, Leaker B D, Lee J E, Nam R and Naguib H E 2019 Shape programming of polymeric based electrothermal actuator (ETA) via artificially induced stress relaxation *Sci. Rep.* 9 11445
- [15] Wang C W, Wang Y B, Yao Y G, Luo W, Wan J Y, Dai J Q, Hitz E, Fu K and Hu L B 2016 A solution-processed high-temperature, flexible, thin-film actuator Adv. Mater. 28 8618–24
- [16] Ahn J et al 2020 Heterogeneous conductance-based locally shape-morphable soft electrothermal actuator Adv. Mater. Technol. 5 1900997
- [17] Song S H, Lee J Y, Rodrigue H, Choi I S, Kang Y J and Ahn S H 2016 35 Hz shape memory alloy actuator with bending-twisting mode Sci. Rep. 6 21118
- [18] Wang D, Li L, Zhang B, Zhang Y F, Wu M S, Gu G Y and Ge Q 2020 Effect of temperature on the programmable

- helical deformation of a reconfigurable anisotropic soft actuator *Int. J. Solids Struct.* **199** 169–80
- [19] Wang T Y, Ge L S and Gu G Y 2018 Programmable design of soft pneu-net actuators with oblique chambers can generate coupled bending and twisting motions Sens. Actuator A 271 131–8
- [20] Hu J, Li X, Ni Y, Ma S D and Yu H F 2018 A programmable and biomimetic photo-actuator: a composite of a photo-liquefiable azobenzene derivative and commercial plastic film J. Mater. Chem. C 6 10815–21
- [21] de Haan L T, Verjans J M N, Broer D J, Bastiaansen C W M and Schenning A P H J 2014 Humidity-responsive liquid crystalline polymer actuators with an asymmetry in the molecular trigger that bend, fold, and curl J. Am. Chem. Soc. 136 10585–8
- [22] Grinberg I, Maccabi N, Kassie A and Elata D 2017 A piezoelectric twisting beam actuator *J. Microelectromech.* Syst. 26 1279–86
- [23] Wang M, Lin B P and Yang H 2016 A plant tendril mimic soft actuator with phototunable bending and chiral twisting motion modes *Nat. Commun.* 7 13981
- [24] Finio B M and Wood R J 2011 Optimal energy density piezoelectric twisting actuators 2011 IEEE/RSJ Int. Conf. Intelligent Robots and Systems pp 384–9
- [25] Gorissen B, Chishiro T, Shimomura S, Reynaerts D, De Volder M and Konishi S 2014 Flexible pneumatic twisting actuators and their application to tilting micromirrors *Sens.* Actuator A 216 426–31
- [26] Han Y W and Dong J Y 2017 High-resolution direct printing of molten-metal using electrohydrodynamic jet plotting *Manuf. Lett.* 12 6–9
- [27] Han Y W and Dong J Y 2018 Fabrication of self-recoverable flexible and stretchable electronic devices J. Manuf. Syst. 48 24–29
- [28] Han Y W and Dong J Y 2018 Electrohydrodynamic (EHD) printing of molten metal ink for flexible and stretchable conductor with self-healing capability Adv. Mater. Technol. 3 1700268
- [29] Cao Y and Dong J Y 2019 High-performance low-voltage soft electrothermal actuator with directly printed micro-heater Sens. Actuator A 297 111546
- [30] Cao Y and Dong J Y 2021 Self-sensing and control of soft electrothermal actuator *IEEE/ASME Trans. Mechatron*. 26 854–63
- [31] Cao Y and Dong J Y 2021 Programmable soft electrothermal actuators based on free-form printing of the embedded heater Soft Matter 17 2577–86